



Article

The Efficient Removal of Methylene Blue Dye Using CuO/PET Nanocomposite in Aqueous Solutions

Suhad Abdulrahman Yasin ^{1,*}, Samie Yaseen Sharaf Zeebaree ², Aymn Yaseen Sharaf Zeebaree ²,
Osama Ismail Haji Zebari ³ and Ibtisam Abdulmajeed Saeed ⁴

- ¹ Chemistry Department, College of Science, University of Duhok, Dahuk 42001, Kurdistan Region, Iraq
² Department of Medical Lab. Technology, Shekhan Technical College of Health, Duhok Polytechnic University, Dahuk 42001, Kurdistan Region, Iraq; samie.yasin@dpu.edu.krd (S.Y.S.Z.); aemanzebari2002@gmail.com (A.Y.S.Z.)
³ General Science Department, Faculty of Education, Soran University, Soran 44008, Kurdistan Region, Iraq; osama.haji@gsci.soran.edu.iq
⁴ Physics Department, College of Science, University of Duhok, Dahuk 42001, Kurdistan Region, Iraq; ibtisamsaid@uod.ac
* Correspondence: suhad.yasin@uod.ac

Abstract: The present research investigates the application of the green method to produce nanocomposites. The CuO/PET fiber nanocomposite can be prepared in two ways. The first way involves the application of the electrospinning technique by which waste plastic cups of polyethylene terephthalate (PET) are converted into nanofibers. In the second way, the copper nanoparticle (CuONPs) is synthesized with the natural capped plant extract of sumac (*Rhus Coriaria* L., family Anacardiaceae) and the CuONPs are then combined as a filler with the PET nanofiber using a cross-linked solvent. The X-ray diffraction (XRD), transmission electron microscopy (TEM), field emission scanning electron microscopy (FESEM), energy dispersion spectroscopy (EDS), and map elements distribution can be applied to investigate the surface modification and alteration of the composite nanofiber morphology. The collected data show that the produced CuO/PET nanocomposites have a high surface area, well distribution of elements, magnificent shape, and stable dispersion state. Furthermore, the CuO/PET nanocomposites are considered as an efficient photocatalytic removal of the toxic methylene blue dye (MB) in aqueous solutions. The results of the present study demonstrate that the photocatalytic efficiency for removing MB dye is achieved in a short time using a low-intensity irradiation ultraviolet light.



Citation: Yasin, S.A.; Sharaf Zeebaree, S.Y.; Sharaf Zeebaree, A.Y.; Haji Zebari, O.I.; Saeed, I.A. The Efficient Removal of Methylene Blue Dye Using CuO/PET Nanocomposite in Aqueous Solutions. *Catalysts* **2021**, *11*, 241. <https://doi.org/10.3390/catal11020241>

Academic Editor: Roberto Comparelli
Received: 19 December 2020
Accepted: 3 February 2021
Published: 11 February 2021

Keywords: CuO; PET; nanocomposite; electrospinning; photocatalytic; methylene blue

Publisher's Note: MDPI stays neutral with regard to jurisdictional claims in published maps and institutional affiliations.



Copyright: © 2021 by the authors. Licensee MDPI, Basel, Switzerland. This article is an open access article distributed under the terms and conditions of the Creative Commons Attribution (CC BY) license (<https://creativecommons.org/licenses/by/4.0/>).

1. Introduction

Nanocomposites are known as the result of binding two different components in a nanoscale with a distinctive physical and chemical behavior. Binding various materials not only integrate their properties but also produce a new different effect and decrease the limitation features of the single species. The composite nanoparticles have significant application prospects in some major industrial fields, such as manufacturing new functional materials, utilizing a new source of energy effectively, remediating wastewater, and introducing new applications in the biomedicine and food industries [1]. The use of heterogeneous semiconductors nanocomposite as photocatalyst and photoelectrocatalytic has opened an important window on the area of water remediation. Researchers have exerted more efforts to enhance the mechanical properties and surface functions of nanocomposites through embedding nanofibers into the metal nanoparticles.

Further, nanocomposite makes it in contact with an electrolyte to create a junction semiconductor/electrolyte interface, which determines the electron-hole separation kinetics and eventually increases the effectiveness and efficiency [2–5]. Nowadays, electrospinning

is the most promising method for synthesizing nanofibers. Electrospinning has proved to be an excellent technology that can be applied to produce polymer fibrous materials with diameters extending from tens to several microns of nanometers. Nanofibers can be used in many applications such as drug delivery, catalyst and biomedicine applications, tissue engineering, environmental engineering, food industry, bioengineering, and water remediation [6–11]. polyethylene terephthalate polymer (PET) is one of the most extensive waste polymeric materials that can be recycled. It has a wide range of applications as in the manufacturing of water drinking cups. Being single-use liquid plastic containers, water drinking cups have become the biggest widespread waste in the environment as a non-biodegradable substance. In a previous study, a PET nanofiber was produced from the wasted PET cups and was tested to evaluate its properties as a high surface area material and its capability as a ready embedding mat [12]. PET can be mixed with metal nanoparticles to produce nanocomposites with efficient physic-chemical properties. There have been innumerable publications related to the synthesis of metal nanoparticles in many research areas. Metal nanoparticle has drawn a considerable amount of attention as an attractive material for researches and innovations. The present research shows that Cu and (CuOx) nanoparticles specifically differ from all other metals due to their significant properties as being efficient, harmless, inexpensive and environmentally friendly. Copper (Cu) and copper oxide (CuOx) nanoparticles can be used in a wide diversity of industrial fields, including chemical manufacturing, energy conversion, energy storage, biological applications, environmental technology, catalytic activity as well as fillers in the PET matrix [13–17]. They can significantly alter the physic-chemical properties of the host polymeric compounds compared to the pristine. Many approaches and applications have been utilized to synthesize metal nanoparticles. Most of these approaches and applications are expensive, chemicals-consuming, and environmentally harmful. More recently, the synthesis of metal nanoparticles using the green method has emerged as an efficient application and has been welcomed by scientists and researchers. Many researchers use plant extracts as a reducing agent for the synthesis of metal nanoparticles. These extracts exhibit a high degree of efficiency due to their availability, harmlessness, sustainability, and the bioactive substances in their composition [18–20]. Sumac, (*Rhus Scoriaria* L., family Anacardiaceae), widely grows in many countries such as Iran, Afghanistan, along the Mediterranean coastline, and the Canary Islands. It is one of the plant substances that can be used in the green production of metal nanoparticles. It comprises many bioactive materials in its structure like hydrolysable, flavonols, phenolic acids, anthocyanins, tannins and other organic acids such as tartaric, malic and citric acids. These compounds have excellent potential for reducing copper ions into copper with zero valence and eventually obtaining the copper nanoparticles [21,22].

Due to the increasing demand for textile goods around the globe, most of the textile industries have increased their production to meet the global demand which in turn has led to the release of large quantities of contaminants into the environmental system of surface water, soil, and sediments. Organic dyes make a sizable portion of these pollutants. They are undegradable by microorganisms and have a noticeable toxic influence on the organisms and the aquatic system [23,24]. Methylene blue dye is a heterocyclic compound used in textile factories. Despite its industrial benefits, it causes many environmental problems due to its accumulation and high toxicity [25].

This study attempts to apply the process of photocatalytic degradation as one of the potential applications for removing dyes and converting the huge organic compounds to small molecules. The process includes exposing semiconductor surface to irradiation light ($h\nu \geq E_g$) which leads to the production of electron/hole pairs (e^-/h^+) by raising an electron from the valence band to the conduction band [26]. Nanocomposites show a high activity for the degradation of the organic substance [27]. Many nanofibers have been generated and composited with a metal nanoparticle to be used for the photodegradation of organic dyes [28–31]. However, the use of most nanofibers suffers from throwbacks due to their high cost, time-consumption, and high-power irradiation.

In this research, the natural capped CuO nanoparticles are synthesized using a plant extract as a reducing and capping agent. A PET nanofiber is produced by the electrospun of the wasted PET polymer. In the next step, CuO nanoparticles are cross-linked on the surface of the electrospun PET nanofiber in order to enhance the dye adsorption. To support the degradation process, the produced nanocomposite is used in the process of photodegradation of the methylene blue dye (MB). Many parameters are investigated to optimize the degradation process including pH, time, and initial concentration. Additionally, the kinetic reaction is put under observation to determine the rate of reaction. The study reveals that an eco-friendly, cheap, sustainable, and effective nanocomposite can be produced in this process and the efficiency of the dye removal is above 99% in 30 min.

2. Results and Discussion

2.1. X-ray Diffraction (XRD) Analysis

The nature of the obtained CuO/PET nanocomposite (phase and size) was examined with the XRD spectrum analysis and compared with the prepared PET nanofiber and CuONPs independently, as shown in Figure 1. The XRD analysis for the prepared CuO/PET nanocomposite revealed a prominent broad peak at location of 2θ (21.12°) back to the PET nanofiber, and two sharp peaks at 36.22°, 43.10° attributed to the presence of the copper oxide nanoparticles (CuONPs) that spread over the PET surface. As the formatted material was closer to amorphous, it became then difficult to calculate the size of the PET particles with the Debye-Scherrer equation. The peak at (15–20) represents the polyester molecules.

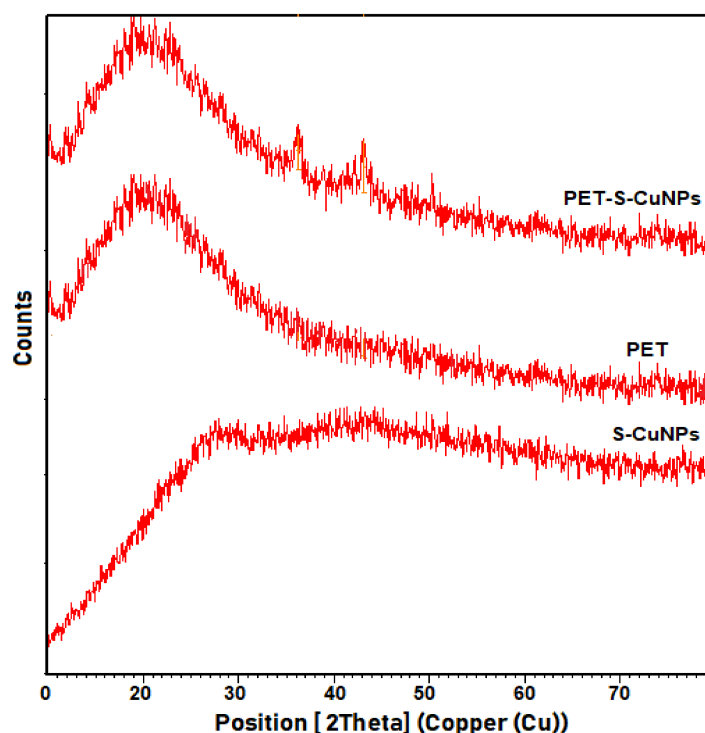


Figure 1. XRD analysis of the CuONPs, PET nanofiber and CuO/PET nanocomposite.

This data is in a close alignment with the work investigated by Mehdi et al. [32,33]. This is attributed to the stretched PET chains which are solidified rapidly after extension, preventing the crystal formation in the electrospun PET nanofibers known for their slow crystallization [34,35]. On the other hand, the two values in the XRD line of the CuO/PET nanocomposite are attributed to the particle size of the CuONPs that distinguishes the surface of the PET nanofiber. The particle size is calculated using Scherrer's law ($D = k\lambda / \beta \cos\theta$), where k , λ , β , and θ represent 0.94 constant value, X-ray wavelength, peak half-width, and Bragg angle half with a size ranging from 4–9 nm. The clarity of the peaks'

positions of CuO/PET nanocomposite prepared from both CuONPs and PET nanofiber is an indication of the occurrence of the adhesion and cohesion processes of the well-prepared polymer components.

2.2. Field Emission Scanning Electron Microscope (FESEM) Analysis

The morphology of the synthesized CuO/PET nanocomposite from the ligation of both PET nanofiber and CuONPs was observed using the FESEM micrograph (Figure 2a–c). The selected nano sizes were calculated by J-image program. The microscopic examination (Figure 2a) clearly showed the CuONPs formation in a spherical agglomeration shape with sizes ranging from 9 to 13 compared to the 100 nm of the pre-prepared PET (Figure 2b) with a lattice shape. Figure 2c demonstrates that the link between the PET nanofiber and CuONPs is created after the formation of CuO/PET composite by glutaraldehyde as a binding agent. This in turn produces a stable network surface covered by the spherical Cu nanoparticles with a clear surface decoration.

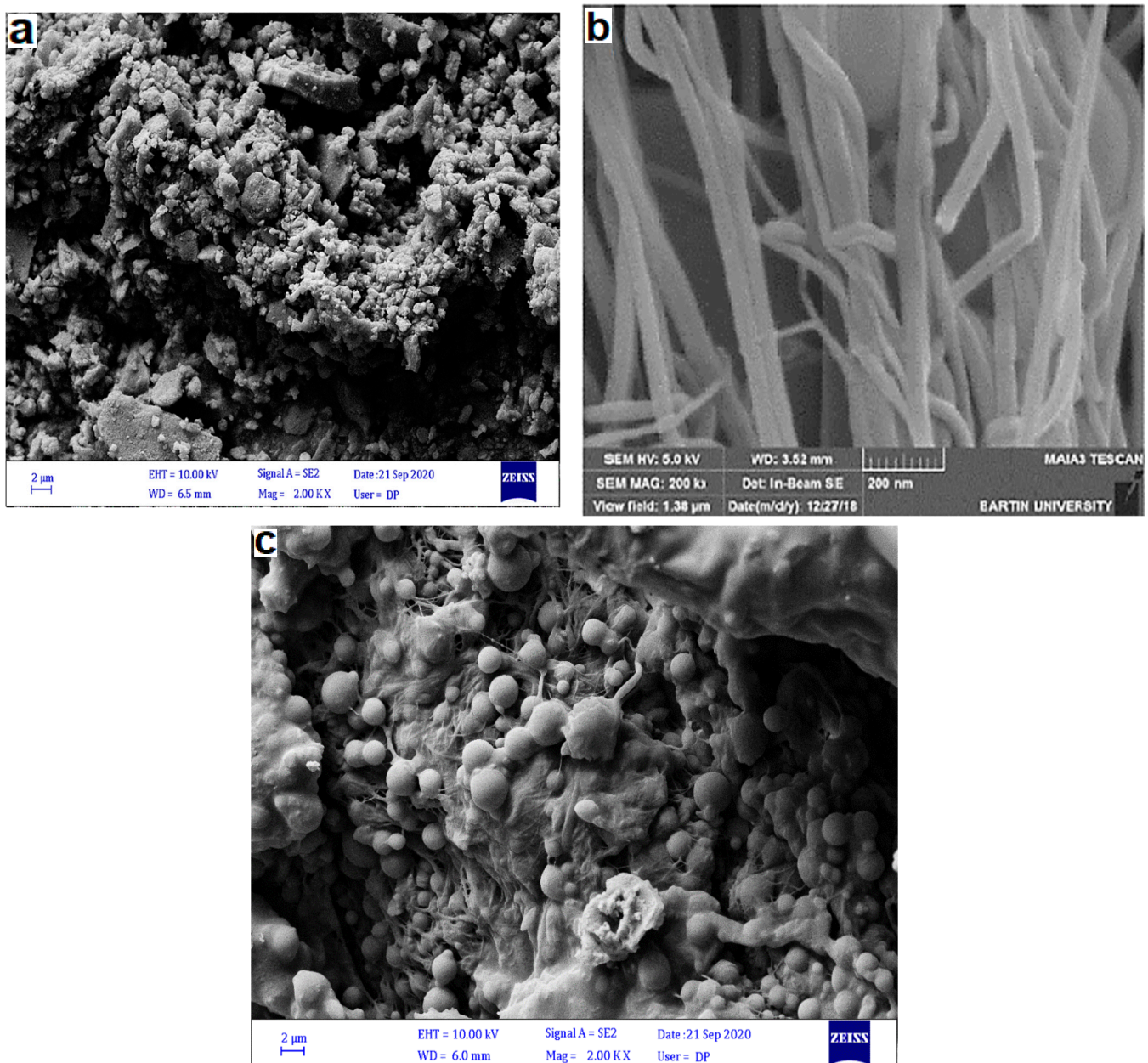


Figure 2. FESEM images of (a) CuONPs, (b) PET nanofibers, and (c) CuO/PET nanocomposite.

2.3. High-Resolution Transmission Electron Microscope (HR-TEM) Analysis

The HR-TEM measurement helps to visualize the size, morphology, and structure of the particles as well as the inherent matrix of the individual CuO/PET nanocomposite obtained from the process of combining CuONPs and PET. The images (Figure 3a,b) of the HR-TEM analysis at the scale bar 200 nm confirm the CuONPs and CuO/PET nanocomposite formation. The image (Figure 3a) shows that CuONPs are formed in a spherical shape with sizes ranging from 7 to 11 nm. Similarly, Figure 3b shows that the CuO/PET nanocomposite combines both traits of CuONPs and PET nanofiber with the assistance of glutaraldehyde as a cross-link agent and with a size range of 7 to 10 nm. The spherical particles spreading individually over the surface of the nanofiber are a further evidence of the correct formation of the composite. This closely matches the results of the obtained FESEM and XRD.

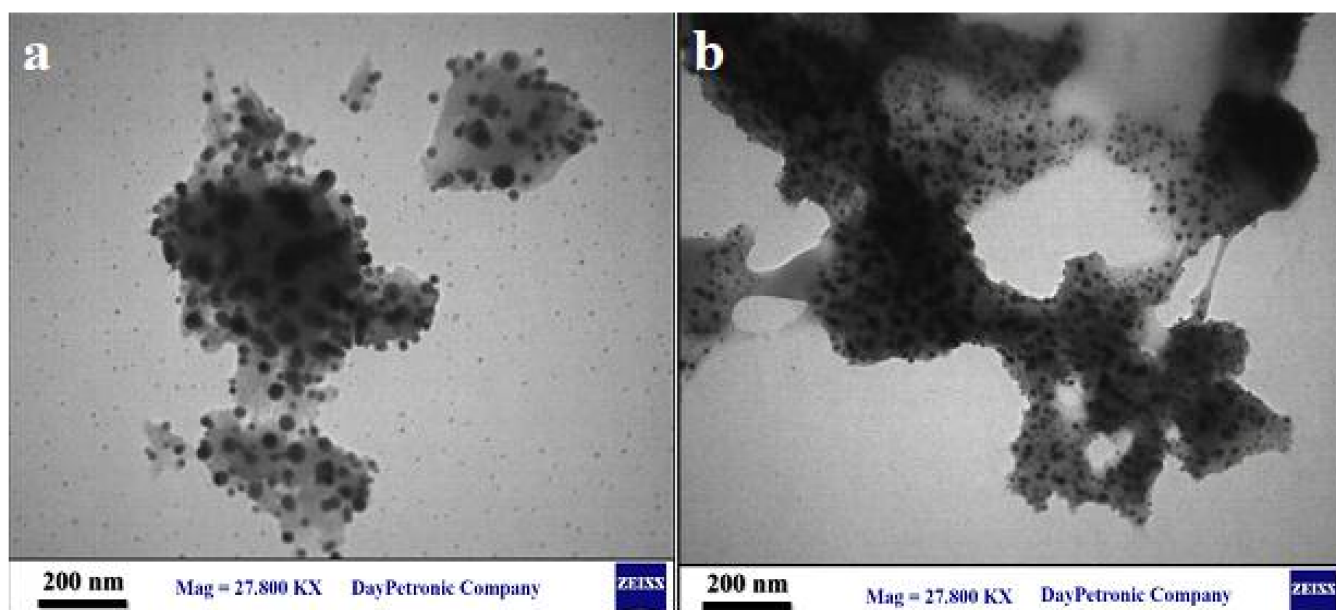


Figure 3. HR-TEM images of (a) CuONPs and (b) CuO/PET nanocomposite.

2.4. Energy-Dispersive Spectroscopy Analysis (EDS) and Elements Distribution Mapping (EDM)

The energy-dispersive spectroscopy analysis (EDS) is conducted in this study to measure the ratio of the existing elements in the CuONPs, PET nanofibers and CuO/PET nanocomposite as shown in Figure 4a–c. The obtained results reveal that the prepared CuONPs contain 37.5% carbon, 17.4% oxygen, and 45.2% copper only (Figure 4a). At the same time, PET includes 88.4% carbon and 11.6% oxygen only (Figure 4b), whilst the CuO/PET nanocomposite only has carbon, oxygen, and copper (Figure 4c). The disparity percentage of PET composition is attributed to the solvent effect. The absence of other elements in the three synthesized nanomaterials and especially in CuO/PET nanocomposite is an indication of the purity of the preparation process. Moreover, the homogeneous distribution provides a better efficiency of the nanocatalyst. The double rise in the percentages of carbon and oxygen and the constant percentage of copper clearly indicate the purity of the of CuO/PET nanocomposite. However, the occurrence of the integrated cohesion of the PET and CuONPs components must be accounted for.

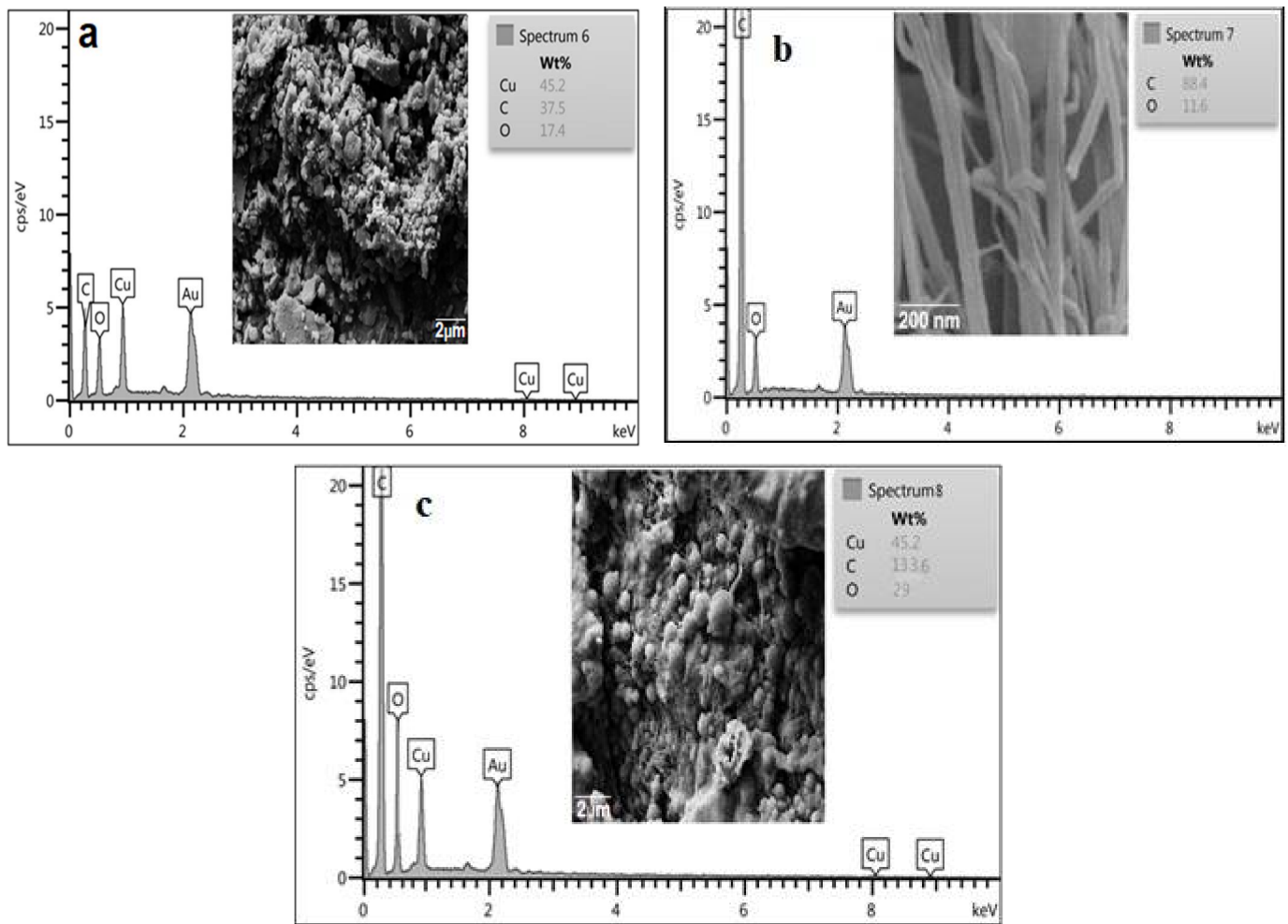


Figure 4. EDS analysis of (a) CuONPs, (b) PET nanofiber and (c) CuO/PET nanocomposite.

Figure 5a–c shows the particle distribution with the mapping diffusion positions of the elements in the corresponding FESEM micrographs of CuONPs, PET nanofiber, and CuO/PET nanocomposite. The diagram reveals the precise distribution of the copper particles in an excellent distance. The present results give another evidence for the existence of the aforementioned materials with the FESEM and EDS measurements emphasizing the purity of the preparation process.

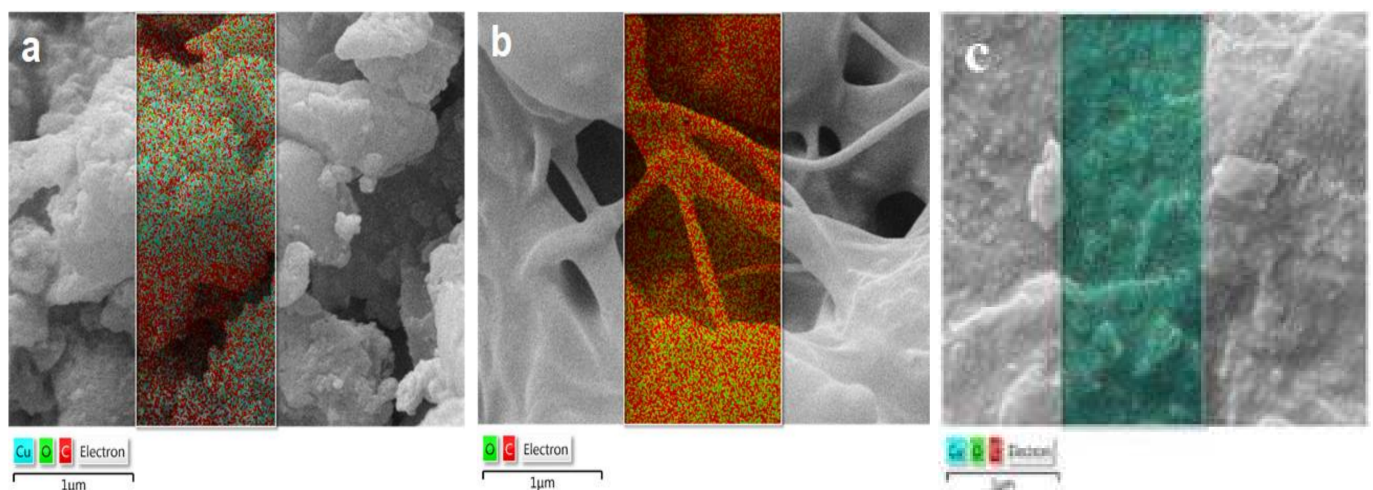


Figure 5. Map distribution of elements (a), CuONPs, (b) PET nanofibers, and (c) CuO/PET nanocomposite.

2.5. Photodegradation Study of MB Dye

The effectiveness of the fabricated CuO/PET nanocomposite is evaluated against the polluted organic methylene blue (MB) dye in an aqueous solution in order to verify its performance and compare it with the previously prepared and measured nanofiber PET performance. The photodegradation experiment was conducted by adding the composite to 5 mL of the MB dye solution (10 ppm). The components of the reaction were magnetically stirred at 500 rpm for 30 min in a dark place to attain the adsorption-desorption equilibrium. After that, the solution was irradiated with a UV lamp (10 Watt) and magnetically stirred continuously. In five-minute intervals, an aliquot (2 mL) was taken out in a glass cuvette to be measured in the UV-vis spectrophotometer in order to record the dye degradation absorbance. The advantage of employing the UV light was to produce the electron and hole pair (e^-/h^+) with a high energy state which migrated to the CuO/PET nanocomposite surface to initiate a wide range of chemical reactions [36]. During a five-minute interval, the blue color intensity of the MB dye solution gradually disappeared and the solution became colorless with the UV light continuously irradiating. This was due to the combination and increase of the CuO/PET active sites and the rise of the efficiency in the degradation of the dye compared to the PET nanofiber individually, as shown in Figure 6a–c. Figure 6a,b presents the recorded absorbance values. It reveals that the maximum removal percentage of MB dye by CuO/PET nanocomposite is 56.5% and 77.5% at 5 and 10 min respectively (Figure 6c–d). In contrast, the previously prepared PET was 0% and 56% in the same conditions. As for the time factor, it was found that the photodegradation activity of the CuO/PET nanocomposite against the dye was faster and ended up within 30 min with a 99% decolorization compared to that of the PET solution which ended at 100 min with 94%. The obtained results were compared with those of our previous study including the results of mixing pomegranate leaves with copper ions and PET solution [12]. The CuO/PET nanocomposite showed higher removal efficiency and effectiveness. The first reason may be attributed to the preparation method. The previous method involved mixing the precursors in one vessel. While, in the current work, they prepared separately then mixed. The second reason is the distribution of copper ions and plant components inside and outside the polymer, thus reducing the pores or active sites responsible for removing the dye. The present method involves decorating the polymer's outer surface by the process of binding which makes it more preferable. In addition, the efficiency of CuO/PET in higher dye decomposition is compared to that highlighted by the other related research studies using nanofibers as a dye removal agent (Table 1). The data indicate that the prepared CuO/PET nanocomposite showed higher removal capacity of MB with less time and lower irradiation intensity compared to the capacity features of CuO/PET nanocomposite in other studies.

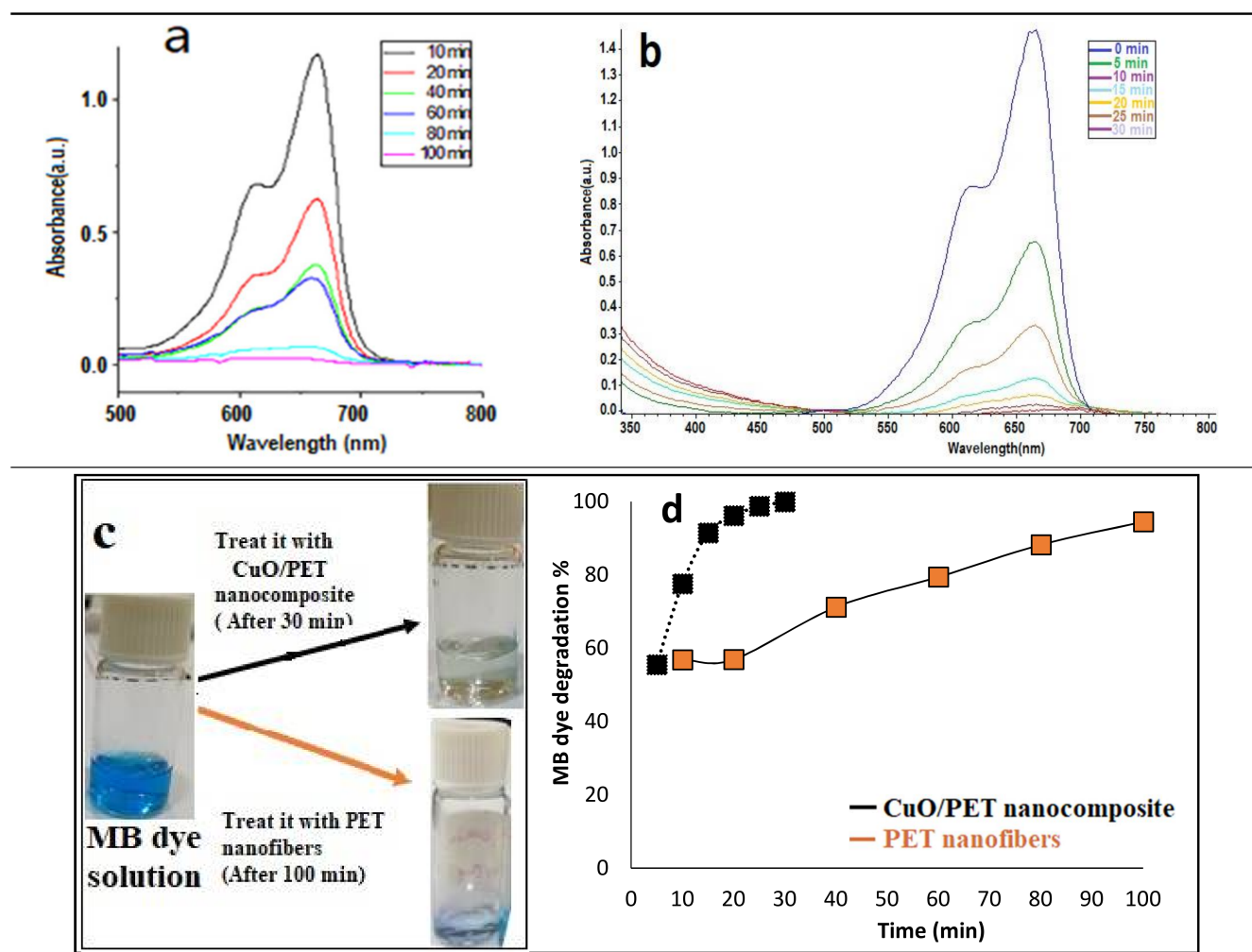


Figure 6. (a,b) are photodegradation MB absorbance by PET nanofiber and CuO/PET nanocomposite, whereas (c,d) are MB dye removal% by PET nanofibers and CuO/PET nanocomposite.

Table 1. Comparison of CuO/PET nanocomposite with PET nanofibers and other related in MB degradation.

Adsorbent	Dye Concentration (mg/L)	Irradiation Light Source	Recorded Time (min)	Reference
CNT-embedded hollow TiO ₂	10	UV 800 Watt	70	[37]
CA-CNT/TiO ₂ -NH ₂	10	UV 40 Watt	300	[31]
TiO ₂ Nanoparticles	10	UV 120 Watt	600	[38]
PET nanofiber/CuO nanoparticles	10	UV 100 Watt	60	[12]
PET nanofibers	10	UV lamp 10 W	80	[39]
CuO/PET nanocomposite	10	UV lamp 10 W	30	this work

2.6. The Kinetics of MB Degradation by CuO/PET Nanocomposite

The photocatalytic kinetics of the prepared CuO/PET nanocomposite are studied via monitoring the degradation of MB dye solution. Figure 7a presents a diagram of C/C_0 versus irradiation time. It was found that the photocatalytic degradation performance of

the CuO/PET nanocomposite against dye was better than that of the PET nanofibers and in high rate. The reaction rate of the dye photodegradation experiment was calculated using the pseudo-first order kinetics:

$$\ln(C_0/C) = kt \quad (1)$$

where C_0 is the initial concentration of MB dye, C is the measured concentrations of the dye degradation at different irradiation times, and kt is the reaction rate of the MB dye decomposition.

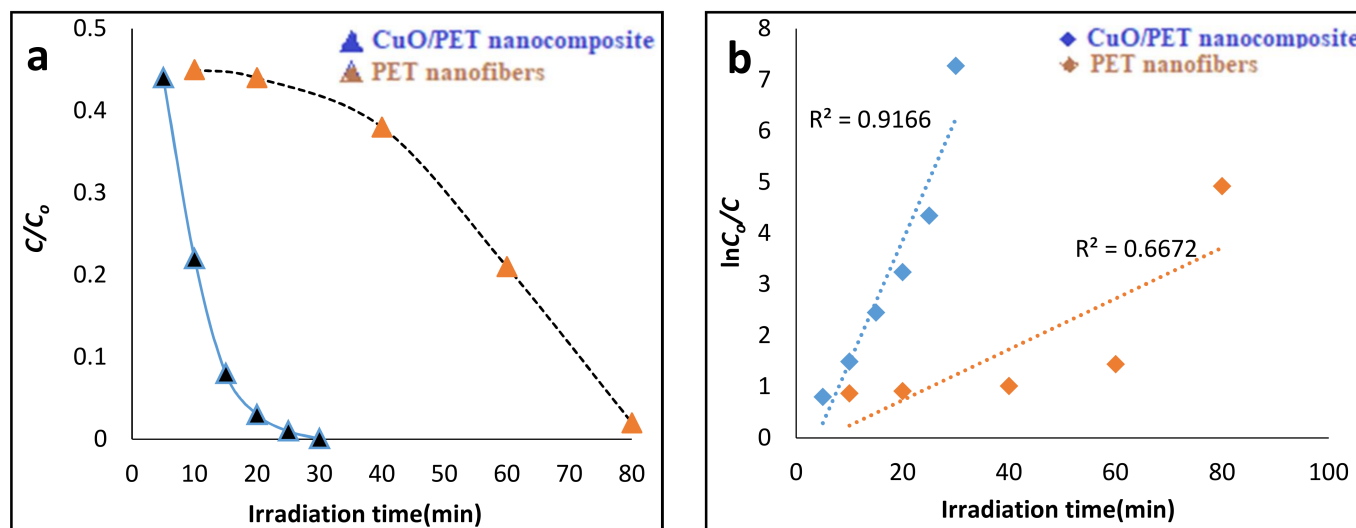
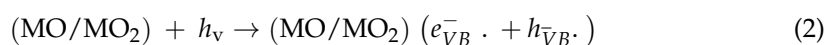


Figure 7. Influence of contact time on MB removal efficiency by PET nanofiber (a) and CuO/PET nanocomposite (b) Fitting of pseudo-first-order of PET nanofiber and CuO/PET nanocomposite.

The diagram in Figure 7a exhibits a good linear curve for the catalyst used in the process of dye removal during a short period of time compared to the PET nanofiber. The catalyst linear curve presents the high activity of the CuO/PET nanocomposite. The constant reaction rate was calculated and recorded according to Figure 7b. The graph of $\ln(C_0/C)$ versus t in Figure 7b shows that the calculated reaction rate (k) for the PET nanofibers was 0.049 min^{-1} , whereas that of the CuO/PET was 0.238 min^{-1} . The obtained k value for the CuO/PET perfectly follows the pseudo-first-order kinetics in which the conformity of the fitting is indicated by the linear regression value ($R^2 = 0.921$) compared to that of the PET nanofiber ($R^2 = 0.667$). The obtained result for the catalyst is acceptable and agrees with the previous reports [3].

The photodecomposition of MB dye in the solution starts with the photoexcitation of the CuO nanoparticles as a semiconductor in which the electron-hole pair on the surface of the CuO catalyst is produced (Equation (2)). The high oxidative capability of the hole ($h + VB$) in the catalyst enables the organic dye (MB) to be instantly oxidized into reactive intermediate molecules (Equation (3)).

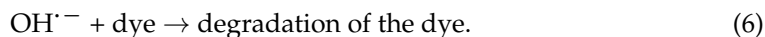
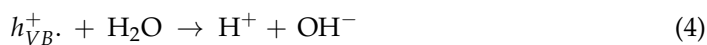


Metal oxide



Furthermore, the hydroxyl radical (OH^\cdot) is considered as another reactive intermediate molecule which is responsible for the decomposition and is produced via water decomposition (Equation (4)). However, it can also be produced through the reaction of the hole with OH^- (Equation (5)). Owing to its features for being influential, nonselective

oxidant ($E^\circ = +3.06$ V), and hydroxyl radical (OH^\bullet), it can work as a fractional or complete mineralizer of many organic chemicals (Equation (6)) [33].



2.7. Influence of pH and MB Dye Concentration on Photodegradation

The effect of the pH on the photodegradation reaction medium is investigated due to its essential and critical role in the decomposition of the organic matters [33]. The results in Figure 8 show that the photolysis of the MB dye increases with the increase in the pH value of the reaction medium. The MB dye increase demonstrates the role and type of the medium in which the dye is mainly degraded. Besides, this medium promotes the formation of the hydroxyl (OH^\bullet) radicals which are considered as robust oxidizing species responsible for raising pH value during dye photodecomposition. Further, the influence of the concentration on the rate of the photocatalytic degradation was examined at various initial MB dye concentrations. It was reported that with the increase in the initial concentration of MB dye, the rate of the degradation dropped down. The decrease in the degradation rate was attributed to the rise in the concentration and the number of dye molecules to be degraded with the other factors such as the rate of the (OH^\bullet) radical generation, nanocomposite dose, dissolved oxygen, light intensity, and time remained constant during the process. Hence, the increase in the initial concentration leads to the decrease of the photocatalytic process [40].

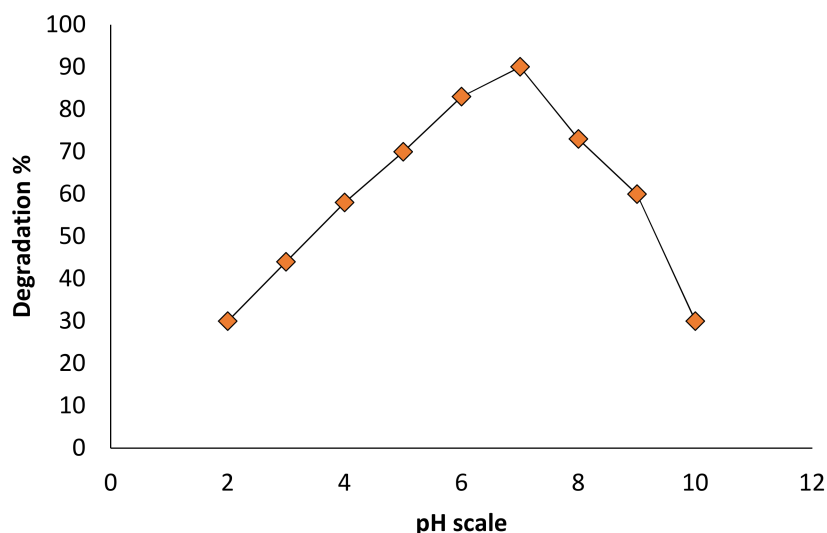


Figure 8. pH influence on degradation of MB dye by CuO/PET nanocomposite.

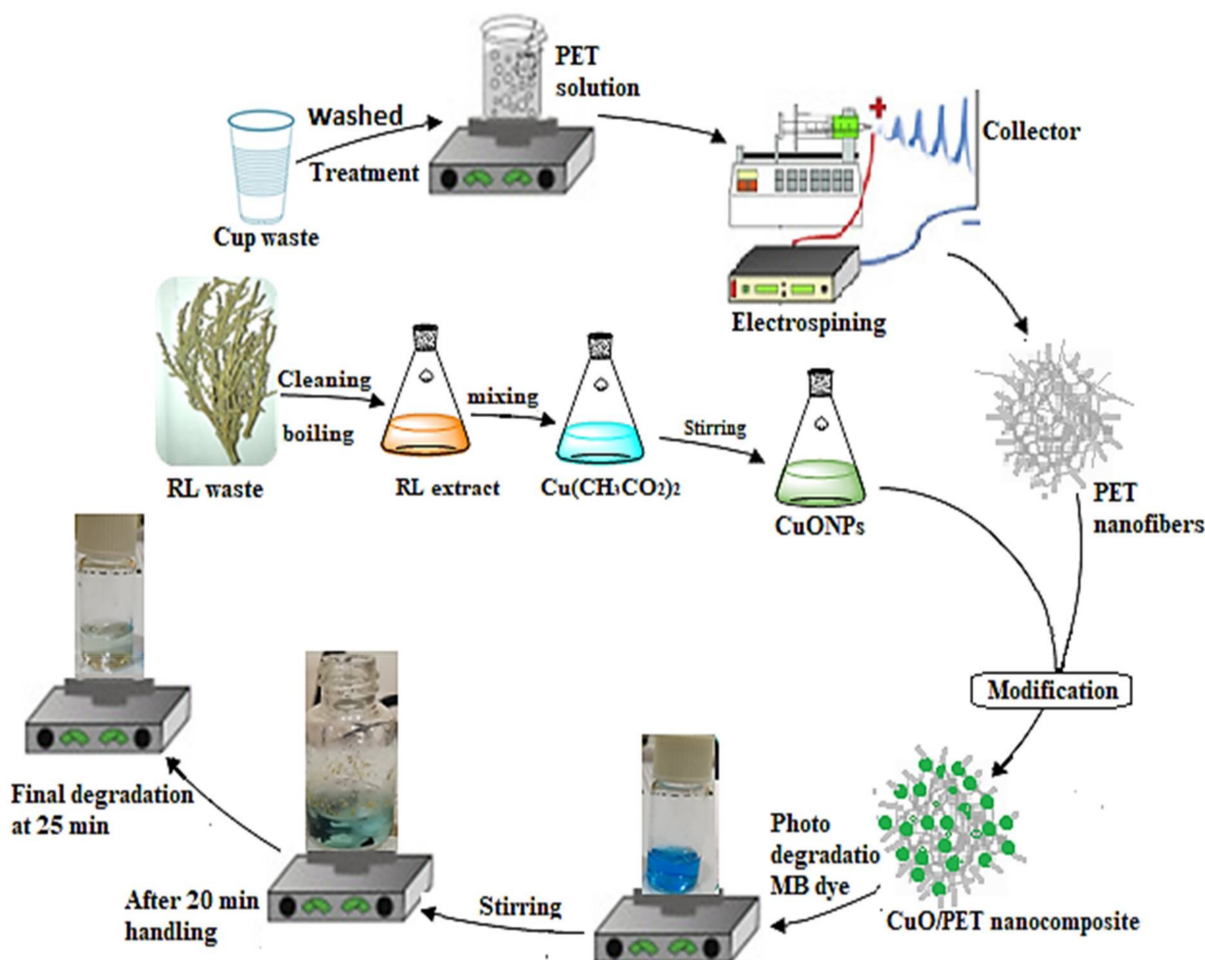
3. Materials and Methods

Fresh green stems of *Rhuscoriaria L* (Sumac) plant were collected from Charboot village-Zebar region/Akre/Kurdistan of Iraq. All chemicals and solvents were purchased from Sigma-Aldrich comp with no purification.

3.1. Preparation of *Rhuscoriaria L* Stems Extract

The stems of *Rhuscoriaria L* were collected and washed with distilled water then dried under sunlight (Scheme 1). The stems were crushed into a fine powder using a mortar. Twenty grams of the powder was added to 200 mL distilled water in the conical flask. The mixture was stirred and heated to 60 °C for 30 min. The waste stems were separated,

and the extract was centrifuged with 4000 rpm for 20 min and filtered with (Whatman No.1). The obtained clear yellow extract was used to reduce the copper ions.



Scheme 1. Steps of CuO/PET nanocomposite preparation and MB dye degradation process.

3.2. Synthesis of Copper Nanoparticles CuONPs

In the separator funnel, 75 mL of the stem extract was added slowly with continuous stirring to the 50 mL 0.1 M of copper acetate solution in the conical flask. The mixture was boiled at 60 C for 30 min. After that, the mixture resulted from the reaction was left in a dark place for 24 h (Scheme 1).

3.3. Preparation of PET Nanofiber

As a wasted material, the PET polymer was collected, washed with a deionized water, and then dried. The electrospun solution was prepared via mixing 3:1 ration of dichloromethane (DCM) and trifluoroacetic acid (TFA). The solution was stirred at room temperature for (4 h) then transferred into a (500 μ L) glass syringe attached to stainless steel needle. The electrospun factors were adjusted as follow:

- 1 mL/h flow rate,
- 15 cm distance between the needle tip and the collector,
- 5% PET concentration,
- 15 kV for the operating voltage [12].

3.4. Preparation of CuO/PET Nanocomposite

0.02 gm of PET nanofiber was mixed with 0.02 gm of CuO-NPs powder in 10 mL vials. Next, 1 mL of glutaraldehyde as a cross-link solution and 5 mL distilled water were added to the mixture to enhance the formation of the composite (Scheme 1). The mixture was stirred for 30 min at the ambient temperature. The composite was then isolated, washed with distilled water three times, and dried in the oven at 40 °C for 30 min.

3.5. Characterization Techniques

The morphology of the prepared CuONPs and CuO/PET nanocomposite was identified with the X-ray diffraction (XRD) instrument using Philips PW1730X'pert PRO powder and the X-ray diffractometer with the CuK α radiation ($k = 1.54060 \text{ \AA}^\circ$) at 10 kV and 30 mA. The scans were measured within the angular range of 0° to 80° with a scanning speed of 1.000 min. The shape, size, and the surface nature of the prepared CuONPs and CuO/PET nanocomposites were observed via the field emission scanning electron microscopy (FE-SEM) (ZEISS, Max 60.000 KX) equipped with the energy dispersive spectroscopy (EDS). The high-resolution transmission electron microscopy (HRTEM) technique, type (Jeo 1/JEM 2100) was used to estimate the morphology and size formation of the CuONPs and CuO/PET nanocomposites.

3.6. Degradation Experiment

The photodegradation process of the methylene blue dye (MB) was carried out under the following conditions:

- 1:1 weight ratio of CuO/PET nanocomposite was selected after several optimization experiments then mixed with 5 mL 10 ppm of (MB) dye solution in the 10 mL vial.
- The content was stirred magnetically for 30 min in a dark place to ensure the completion of the adsorption-desorption equilibrium process.
- The component of the reaction was exposed to UV lamp (10 Watt) in which the sample was withdrawn from the vial for a fixed time interval in order to screen the dye degradation using the spectrophotometer.

The following Formula (7) and (8) was used to calculate the percentage of the degradation of MB dye in the aqueous solution:

$$\text{Degradation rate \%} = [C_0 - C/C_0 \times 100] \quad (7)$$

$$\text{Degradation rate \%} = [A_0 - A/A_0 \times 100] \quad (8)$$

where C_0 is the initial concentration of MB dye, C is the MB dye concentration (mg/L) after irradiation at various time points, and A_0 and A are the initial MB dye absorbance before and after irradiation, respectively.

4. Conclusions

In this study, copper nanoparticles (CuONPs) are synthesized by using the sumac stem extracts as a clean, low-cost, and environmentally friendly reducing agent. The copper nanoparticles are embedded with the pre-prepared PET nanofiber in an easy and simple method. The produced CuO/PET nanocomposite reveals a high photocatalytic activity for removing the MB dye (99%) and in a very short period of time (30 min) compared to that of the PET nanofiber. The results show that the photodecomposition of the methylene blue (MB) dye by the CuO/PET nanocomposite is higher and more efficient than that of the PET nanofibers. Moreover, the study results of the degradation kinetics confirm that the activity of the prepared CuO/PET nanocomposite in the elimination of the MB dye from an aqueous solution perfectly follows the pseudo-first-order. The maximum adsorption efficiency of the CuO/PET is attributed to the physical and chemical attraction forces of its components against the MB dye. Furthermore, the characterization results show that the roles of all the components in the CuO/PET nanocomposite are considerably affecting the

degradation efficiency of MB. The nanocomposite shows a rapid degradation rate for MB using a low power intensity source which in turn minimizes the overall costs.

Author Contributions: S.A.Y.: Main idea and results analysis; S.Y.S.Z.: Conceptualization & Writing; A.Y.S.Z.: Writing & Editing; O.I.H.Z.: Writing & Editing; I.A.S.: Supervising engineer. All authors have read and agreed to the published version of the manuscript.

Funding: USAID Partnerships for Enhanced Engagement in Research (PEER) Program.

Data Availability Statement: All data have been put in this paper and there is no supplementary data.

Acknowledgments: The authors are deeply grateful for the financial support offered by USAID Partnerships for Enhanced Engagement in Research (PEER) Program. It is an international grants program that funds scientists and engineers in developing countries in partnership with U.S. government-funded researchers to address global development challenges. It is administered by the U.S. National Academies of Sciences, Engineering and Medicine (NASEM), PEER/Iraq project/cycle 6.

Conflicts of Interest: The authors declare no conflict of interest.

References

1. Melinte, V.; Stroea, L.; Chibac-Scutaru, A.L. Polymer Nanocomposites for Photocatalytic Applications. *Catalysts* **2019**, *9*, 986. [[CrossRef](#)]
2. Morsi, R.E.; Al-Sabagh, A.M.; Moustafa, Y.M.; Elkholy, S.G.; Sayed, M.S. Polythiophene modified chitosan/magnetite nanocomposites for heavy metals and selective mercury removal. *Egypt. J. Pet.* **2018**, *27*, 1077–1085. [[CrossRef](#)]
3. Mohamed, A.M.; El-Sayed, R.; Osman, T.A.; Toprak, M.S.; Muhammed, M.; Uheida, A. Composite nanofibers for highly efficient photocatalytic degradation of organic dyes from contaminated water. *Environ. Res.* **2016**, *145*, 18–25. [[CrossRef](#)] [[PubMed](#)]
4. Kerkeni, L.; Ruano, P.; Delgado, L.L.; Picco, S.; Villegas, L.; Tonelli, F.; Merlo, M.; Rigau, J.; Diaz, D.; Masuelli, M. *Modern Electrochemical Methods in Nano, Surface and Corrosion Science*; Aliofkhaezraei, M., Ed.; InTech: Rijeka, Croatia, 2016; p. 13.
5. Bessegato, G.G.; Guaraldo, T.T.; De Brito, J.F.; Brugnera, M.F.; Zannoni, M.V.B. Achievements and Trends in Photoelectrocatalysis: From Environmental to Energy Applications. *Electrocatalysis* **2015**, *6*, 415–441. [[CrossRef](#)]
6. Wang, S.; Cao, X.; Shen, M.; Guo, R.; Bányai, I.; Shi, X. Fabrication and morphology control of electrospun poly(γ -glutamic acid) nanofibers for biomedical applications. *Colloids Surfaces B: Biointerfaces* **2012**, *89*, 254–264. [[CrossRef](#)]
7. Mohamed, A.; Yousef, S.; Ali AbdelNaby, M.A.; Osman, T.A.; Hamawandi, B.; Toprak, M.S.; Muhammed, M.; Uheida, A. Photocatalytic degradation of organic dyes and enhanced mechanical properties of PAN/CNTs composite nanofibers. *Sep. Purif. Technol.* **2017**, *182*, 219–223. [[CrossRef](#)]
8. Zhang, Y.; Chwee, T.L.; Ramakrishna, S.; Huang, Z.-M. Recent development of polymer nanofibers for biomedical and biotechnological applications. *J. Mater. Sci. Mater. Med.* **2005**, *16*, 933–946. [[CrossRef](#)] [[PubMed](#)]
9. Kriegel, C.; Arrechi, A.; Kit, K.; McClements, D.J.; Weiss, J. Fabrication, Functionalization, and Application of Electrospun Biopolymer Nanofibers. *Crit. Rev. Food Sci. Nutr.* **2008**, *48*, 775–797. [[CrossRef](#)]
10. Podgórski, A.; Bałazy, A.; Gradoń, L. Application of nanofibers to improve the filtration efficiency of the most penetrating aerosol particles in fibrous filters. *Chem. Eng. Sci.* **2006**, *61*, 6804–6815. [[CrossRef](#)]
11. Carpenter, A.W.; De Lannoy, C.-F.; Wiesner, M.R. Cellulose Nanomaterials in Water Treatment Technologies. *Environ. Sci. Technol.* **2015**, *49*, 5277–5287. [[CrossRef](#)]
12. Yasin, S.A.; Abbas, J.A.; Saeed, I.A.; Ahmed, I.H. The application of green synthesis of metal oxide nanoparticles embedded in polyethylene terephthalate nanofibers in the study of the photocatalytic degradation of methylene blue. *Polym. Bull.* **2020**, *77*, 3473–3484. [[CrossRef](#)]
13. Gawande, M.B.; Goswami, A.; Felpin, F.-X.; Asefa, T.; Huang, X.; Silva, R.; Zou, X.; Zbořil, R.; Varma, R.S. Cu and Cu-Based Nanoparticles: Synthesis and Applications in Catalysis. *Chem. Rev.* **2016**, *116*, 3722–3811. [[CrossRef](#)]
14. Bondžić, A.M.; Senčanski, M.V.; Vujačić Nikezić, A.V.; Kirillova, M.V.; André, V.; Kirillov, A.M.; Bondžić, B.P. Aminoalcoholate-driven tetracopper(II) cores as dual acetyl and butyrylcholinesterase inhibitors: Experimental and theoretical elucidation of mechanism of action. *J. Inorg. Biochem.* **2020**, *205*, 110990. [[CrossRef](#)]
15. Astakhov, G.S.; Bilyachenko, A.N.; Levitsky, M.M.; Shul'Pina, L.S.; Korlyukov, A.A.; Zubavichus, Y.V.; Khrustalev, V.N.; Vologzhanina, A.V.; Shubina, E.S.; Dorovatovskii, P.V.; et al. Coordination Affinity of Cu(II)-Based Silsesquioxanes toward N,N-Ligands and Associated Skeletal Rearrangements: Cage and Ionic Products Exhibiting a High Catalytic Activity in Oxidation Reactions. *Inorg. Chem.* **2020**, *59*, 4536–4545. [[CrossRef](#)]
16. Nishi, T.; Sato, S.; Arai, T.; Akimoto, Y.; Kitazumi, K.; Kosaka, S.; Takahashi, N.; Nishimura, Y.F.; Matsuoka, Y.; Morikawa, T. Low-Overpotential Electrochemical Water Oxidation Catalyzed by CuO Derived from 2 nm-Sized Cu₂(NO₃)(OH)₃ Nanoparticles Generated by Laser Ablation at the Air–Liquid Interface. *ACS Appl. Energy Mater.* **2020**, *3*, 8383–8392. [[CrossRef](#)]
17. Oliva-Puigdomènech, A.O.; De Roo, J.; Van Avermaet, H.; De Buysser, K.; Hens, Z. Scalable Approaches to Copper Nanocrystal Synthesis under Ambient Conditions for Printed Electronics. *ACS Appl. Nano Mater.* **2020**, *3*, 3523–3531. [[CrossRef](#)]

18. Yaseen, S.; Zeebaree, S.; Yaseen, A. Synthesis of copper nanoparticles as oxidising catalysts for multi-component reactions for synthesis of 1,3,4- thiadiazole derivatives at ambient temperature. *Sustain. Chem. Pharm.* **2019**, *13*, 100155. [[CrossRef](#)]
19. Yaseen, S.; Zeebaree, S.; Yaseen, A.; Ismail, O.; Zebari, H. Diagnosis of the multiple effect of selenium nanoparticles decorated by *Asteriscus graveolens* components in inhibiting HepG2 cell proliferation. *Sustain. Chem. Pharm.* **2020**, *15*, 100210. [[CrossRef](#)]
20. Ismail Haji Zebari, O.; Yaseen Sharaf Zeebaree, S.; Yaseen Sharaf Zeebaree, A.; Ismail Haji Zebari, H.; Abbas, H.R. Anti-bacterial Activity of Copper Nanoparticles Fabricate via Malva Sylvesteris Leaf Extract. *Kurdistan J. Appl. Res.* **2019**, 146–156. [[CrossRef](#)]
21. Shabestarian, H.; Homayouni-Tabrizi, M.; Soltani, M.; Namvar, F.; Azizi, S.; Mohamad, R.; Shabestarian, H. Green Synthesis of Gold Nanoparticles Using Sumac Aqueous Extract and Their Antioxidant Activity. *Mater. Res.* **2017**, *20*, 264–270. [[CrossRef](#)]
22. Ghorbani, P.; Soltani, M.; Homayouni-Tabrizi, M.; Namvar, F.; Azizi, S.; Mohammad, R.; Moghaddam, A.B. Sumac Silver Novel Biodegradable Nano Composite for Bio-Medical Application: Antibacterial Activity. *Molecules* **2015**, *20*, 12946–12958. [[CrossRef](#)]
23. Sivakumar, P.; Palanisamy, P.N. Low-cost non-conventional activated carbon for the removal of reactive red 4: Kinetic and isotherm studies. *Rasayan J. Chem.* **2008**, *1*, 871–883.
24. Yaseen, D.A.; Scholz, M. *Textile Dye Wastewater Characteristics and Constituents of Synthetic Effluents: A Critical Review*; Springer: Berlin/Heidelberg, Germany, 2019.
25. Hassanpour, M.; Safardoust-Hojaghan, H.; Salavati-Niasari, M. Degradation of methylene blue and Rhodamine B as water pollutants via green synthesized Co₃O₄/ZnO nanocomposite. *J. Mol. Liq.* **2017**, *229*, 293–299. [[CrossRef](#)]
26. Hou, C.; Hu, B.; Zhu, J. Photocatalytic Degradation of Methylene Blue over TiO₂ Pretreated with Varying Concentrations of NaOH. *Catalysts* **2018**, *8*, 575. [[CrossRef](#)]
27. Koltsov, I.; Wojnarowicz, J.; Nyga, P.; Smalcz-Koziorowska, J.; Stelmakh, S.; Babyszko, A.; Morawski, A.W.; Lojkowski, W. Novel Photocatalytic Nanocomposite Made of Polymeric Carbon Nitride and Metal Oxide Nanoparticles. *Molecules* **2019**, *24*, 874. [[CrossRef](#)] [[PubMed](#)]
28. Sun, K.; Wang, L.; Wu, C.; Deng, J.; Pan, K. Fabrication of α -Fe₂O₃@rGO/PAN Nanofiber Composite Membrane for Photocatalytic Degradation of Organic Dyes. *Adv. Mater. Interfaces* **2017**, *4*, 1–7. [[CrossRef](#)]
29. Ademola Bode-Aluko, C.A.; Perea, O.; Kyaw, H.H.; Al-Naamani, L.; Al-Abri, M.Z.; Tay Zar Myint, M.; Rossouw, A.; Fatoba, O.; Petrik, L.; Dobretsov, S. Photocatalytic and antifouling properties of electrospun TiO₂ polyacrylonitrile composite nanofibers under visible light. *Mater. Sci. Eng. B* **2021**, *264*, 114913. [[CrossRef](#)]
30. Maeng, S.K.; Cho, K.; Jeong, B.; Lee, J.; Lee, Y.; Lee, C.; Choi, K.J.; Hong, S.W. Substrate-immobilized electrospun TiO₂ nanofibers for photocatalytic degradation of pharmaceuticals: The effects of pH and dissolved organic matter characteristics. *Water Res.* **2015**, *86*, 25–34. [[CrossRef](#)] [[PubMed](#)]
31. Salama, A.; Mohamed, A.; Aboamera, N.M.; Osman, T.A.; Khattab, A. Photocatalytic degradation of organic dyes using composite nanofibers under UV irradiation. *Appl. Nanosci.* **2018**, *8*, 155–161. [[CrossRef](#)]
32. Yasin, S.A.; Abbas, J.A.; Mohamed, M.A.; Saeed, I.A. Data of characterization of electrospun waste polyethylene terephthalate (PET) nanofibers. *Data Brief* **2020**, *30*, 105535. [[CrossRef](#)]
33. Mehdi, M.; Mahar, F.K.; Qureshi, U.A.; Khatri, M.; Khatri, Z.; Ahmed, F.; Kim, I.S. Preparation of colored recycled polyethylene terephthalate nanofibers from waste bottles: Physicochemical studies. *Adv. Polym. Technol.* **2018**, *37*, 2820–2827. [[CrossRef](#)]
34. Hadjizadeh, A.; Aji, A.; Bureau, M.N. Nano/micro electro-spun polyethylene terephthalate fibrous mat preparation and characterization. *J. Mech. Behav. Biomed. Mater.* **2011**, *4*, 340–351. [[CrossRef](#)] [[PubMed](#)]
35. Strain, I.N.; Wu, Q.; Pourrahimi, A.M.; Hedenqvist, M.S.; Olsson, R.T.; Andersson, R.L. Electrospinning of recycled PET to generate tough mesomorphic fibre membranes for smoke filtration. *J. Mater. Chem. A* **2015**, *3*, 1632–1640. [[CrossRef](#)]
36. Alzahrani, E. Photodegradation of Eosin Y Using Silver-Doped Magnetic Nanoparticles. *Int. J. Anal. Chem.* **2015**, *2015*, 1–11. [[CrossRef](#)] [[PubMed](#)]
37. Jung, J.-Y.; Lee, D.; Lee, Y.-S. CNT-embedded hollow TiO₂ nanofibers with high adsorption and photocatalytic activity under UV irradiation. *J. Alloy. Compd.* **2015**, *622*, 651–656. [[CrossRef](#)]
38. Bubacz, K.; Choina, J.; Dolat, D.; Morawski, A.W. Methylene blue and phenol photocatalytic degradation on nanoparticles of anatase TiO₂. *Polish J. Environ. Stud.* **2010**, *19*, 685–691.
39. Yasin, S.A.; Abbas, J.A.; Ali, M.M.; Saeed, I.A.; Ahmed, I.H. Methylene blue photocatalytic degradation by TiO₂ nanoparticles supported on PET nanofibres. *Mater. Today Proc.* **2020**, *20*, 482–487. [[CrossRef](#)]
40. Rayalu, S.S.; Mangrulkar, P.A.; Kamble, S.P.; Joshi, M.M.; Meshram, J.S.; Labhasetwar, N. Photocatalytic Degradation of Phenolics by N-Doped Mesoporous Titania under Solar Radiation. *Int. J. Photoenergy* **2012**, *2012*, 1–10. [[CrossRef](#)]